Science Press

ARTICLE

Nanoflower Copper Sulfide as Cathode Materials for Magnesium Ion Batteries

He Yuantai[1],　Wu Liang[1,2],　Shi Yongan[3],　Zhong Zhiyong[1],　Yao Wenhui[1,2],　Pan Fusheng[1,2]

[1] National Engineering Research Center for Magnesium Alloys, College of Materials Science and Engineering, Chongqing University, Chongqing 400044, China; [2] State Key Laboratory of Mechanical Transmission for Advance Equipment, Chongqing University, Chongqing 400044, China; [3] Chizhou Research Institute of Quality Supervision and Inspection, Chizhou 247100, China

Abstract: CuS-C50, the cathode materials for magnesium ion batteries, was synthesized by adding the surfactant cetyltrimethyl ammonium bromide (CTAB) and adjusting the percentage of ethylene glycol to 50vol% in hydrothermal synthesis process. Results show that CuS-C50 has the complete nanoflower structure. In aluminum chloride-pentamethylcydopentodiene/tetrahydrofuran (APC/THF) electrolyte, the CuS-C50 exhibits a high specific capacity of 331.19 mAh/g when the current density is 50 mA/g and still keeps a specific capacity of 136.92 mAh/g over 50 cycles when the current density is 200 mA/g. Results of morphology characterizations indicate that the complete nanoflower structure can provide more active sites and reduce the barriers for Mg^{2+} movement, eventually improving the charge and discharge performance of the CuS cathode materials for magnesium ion batteries.

Key words: copper sulfide; nanoflower; magnesium ion batteries; CTAB; hydrothermal synthesis

1　Introduction

Under the stimulation of the large demand for electric vehicles, wearable devices and large-scale energy storage, the advanced energy storage batteries have been greatly developed. Metal ion battery is a new type of energy, which is safe, efficient and environmentally friendly, and has great development advantages[1–6]. Among several metal ion batteries, magnesium ion batteries have greater development potential than other metal ion batteries, such as lithium ion batteries, iron ion batteries and sodium ion batteries[7–10]. Magnesium ion batteries can provide more electrons theoretically, and have a larger theoretical specific capacity. Magnesium metal as cathode of batteries is easy to deposit and dissolve, and magnesium cathode is difficult to form dendrites in charge and discharge process[11–13]. In addition, compared with increasingly scarce lithium metal, magnesium metal is more abundant in the earth, which can effectively reduce the production cost of batteries[14]. Magnesium ion batteries have high safety performance and long service life, which are considered as the most likely leader of next-generation batteries systems[15–16]. Unfortunately, although magnesium ion batteries have many advantages, there are still some problems that need to be solved[17]. For example, magnesium ion (Mg^{2+}) leads to an extremely strong polarization, which slows down diffusion of Mg^{2+} into the cathode material[18–19], and there are few active sites for Mg^{2+} to embed in[20–21]. Therefore, the development and application of magnesium ion batteries are restricted.

Cathode materials for magnesium ion batteries mainly include intercalation type material and conversion type material[22–26]. The conversion type cathode materials can absorb and release electrical energy by chemical reaction with Mg^{2+}, which usually have higher theoretical specific capacity, energy and electrochemical reaction platform with smaller polarization[27–30]. Whereas, their actual electrochemical performance is often restricted by other components, such as the electrolyte and diaphragm, as well as the slow transfer of Mg^{2+} in the material and poor interface stability[31–32]. Now, many cathode materials have been used for magnesium ion

batteries, such as MnO_2[33], V_2O_5[34] and TiO_2[35], which are oxides of transition metal; $TiSe_2$[36] and $CuSe$[37], which are selenides of transition metal; TiS_2[38–39], Ti_2S_4[40], VS_4[41] and CuS[42–46], which are sulfides of transition metal. Among these materials, copper sulfide (CuS) exhibits good cycles stability, high specific capacity of 560 mAh/g and high conductivity of 103 S/cm, which is known as an ideal cathode material for magnesium ion batteries. The CuS materials with various structures, such as one-dimensional rods and tubes, two-dimensional sheets and three-dimensional flowers and balls, exhibit good electrochemical properties. Wu et al[47] found that the synthesized CuS nanoparticles exhibit high reversible capacity of 175 mAh/g at a current density of 50 mAh/g with the non-nucleophilic electrolyte ($HMDS_xAlCl_{4-x}^{-}$, $0 \leq x \leq 4$). Shen et al[48] successfully prepared hollow CuS nanocubes whose reversible specific capacity can reach 200 mAh/g at a current density of 100 mA/g, exhibiting high performance in magnesium ion batteries. In addition, Du et al[49] also synthesized mesoporous CuS nanotube with discharge capacity of 281.2 mAh/g at a current density of 20 mA/g. It is worth noting that among these CuS nanostructures, the three-dimensional CuS nanostructure can combine the coupling and synergistic effects and has better charge and discharge performance of magnesium ion batteries because of the large specific surface area which can provide larger active sites for electrochemical reaction[48,50–51]. Moreover, it is reported that the nanostructure of CuS can be effectively enhanced through changing synthesis time, temperature and surfactant. Particularly, the variety of surfactant has significant influence on materials structure. Hence, it is of great significance to design cathode material for magnesium ion batteries with three-dimensional CuS by adjusting the variety of surfactant.

In this study, one special structure CuS, named as CuS-C50, was synthesized by adding the surfactant cetyltrimethyl ammonium bromide (CTAB) and adjusting the percentage of ethylene glycol to 50vol% in hydrothermal synthesis process. The microstructure and composition of CuS-C50 were analyzed before the electrochemical performance testing. And the charge and discharge performance was tested by LAND testing system to explore the cathode materials with high electrochemical performance for magnesium ion batteries.

2 Experiment

In this study, hydrothermal method was used to synthesize the CuS. All chemicals were purchased from Sinopharm Chemical Reagent Co., Ltd and no further purification was required. A certain amount of deionized water and ethylene glycol were dissolved to obtain mixed solution of 80 mL, and the proportion of ethylene glycol was kept at 50vol% in mixed solution. Then, $Cu(NO_3)_2 \cdot 3H_2O$ (4.0 mmol) and CH_4N_2S (8.0 mmol) were dissolved in the solution. Next, CTAB surfactant of 0.4 g was added, and stirred for 30 min. Finally, the mixed solution was poured into the reaction vessel, and the reaction temperature was kept at 100 °C for 20 h. The synthesized CuS was named CuS-C50. Ethylene glycol of 50vol% in the solvent was no longer used, the surfactant was changed to

polyvinyl pyrrolidone (PVP), and the rest of the steps were unchanged. In this case the synthesized CuS was named as CuS-P50. Moreover, without ethylene glycol of 50vol% in the solvent, no surfactant was added, and the rest of the steps were unchanged. This synthesized CuS was named as CuS-50. All synthesized CuS materials were washed more than 3 times with deionized water and ethylene glycol, and dried in a vacuum drying oven for 12 h. The temperature was kept at 60 °C.

The crystal structure of CuS was characterized by X-ray diffractometer (XRD, Rigaku D/MAX-2500X) with Cu Kα ray, and the range was 20°–80°. An X-ray photoelectron spec-troscope (XPS, ESCALAB 250Xi, Thermo Scientific, USA) was used to analyze the chemical structure of CuS. The sur-face structure and morphology composition of the CuS were observed by scanning electron microscope (SEM, JSM-7800F, JEOL, Japan) and transmission electron microscope (TEM, Talos F200S, ThermoFisher Scientific, Netherlands). The glove box (Mbraun, Unilab, Germany, H_2O and $O_2 < 0.1 \times 10^{-4}$ vol%) was used to disassemble cells for testing different charge and discharge states.

Before measuring the charge and discharge performance of CuS, CuS of 80%, super carbon of 10% and polyvinylidene fluoride binder of 10% were ground in quartz mortar for 20 min, and then an appropriate amount of N-methylpyrro-lidone (NMP) was added and stirred for 3 h. Eventually, positive electrode slurry was obtained. The prepared slurry was evenly distributed over the copper foil, and kept in a blast drying oven at 80 °C. After 12 h, take out copper foil and cut into the disc of 12 mm[51]. The electrochemical performance of prepared positive electrode was tested with magnesium metals as counter electrode and reference electrode, glass fiber as separator and aluminum chloride-pentamethylcyclopentadiene/ tetrahydrofuran (APC/THF) as electrolyte. It was worth noting that the assembling process of button battery must be conducted in glove box under an argon atmosphere. The cycle ability and rate capability of the magnesium ion batteries were tested by the LAND testing system, and the testing voltage range was from 0.01 V to 2.00 V. The electrochemical workstation (Brilliance, Shanghai) was used for cyclic voltammetry (CV) test, and the scanning speeds included 0.2, 0.4, 0.6, 0.8, and 1.0 mV/s with the voltage range from 0.01 V to 2.00 V. To identify the corrosion resistance, electro-chemical impedance spectroscopy (EIS) was conducted by the electro-chemical workstation (Princeton PARSTAT 4000A, USA), and the testing frequency was from 10^5 Hz to 10^{-2} Hz. EIS tests were conducted at least 3 times to reduce the experimental errors[52].

3 Results and Discussion

The crystal structure and crystallinity of CuS-C50 were characterized by XRD, as shown in Fig.1a. It can be seen that characteristic peaks of CuS-C50 are matched well with the standard card (JCPDS No. 06-0464) and no diffraction peak appears, indicating that the synthesized CuS-C50 has very high purity. The element valence states and composition of
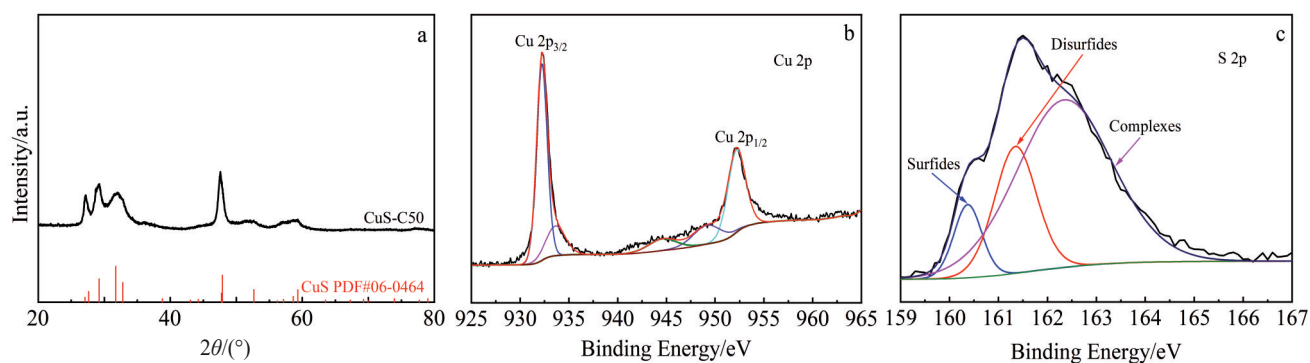
Fig.1 XRD patterns of CuS-C50 (a); XPS spectra of Cu 2p (b) and S 2p (c)

CuS-C50 are shown in Fig. 1b – 1c. XPS results indicate that there are two strong peaks of Cu $2p_{1/2}$ and Cu $2p_{3/2}$ which are presented at 932.1 and 952.1 eV, respectively. It can be speculated that it is related to the Cu^{2+} in CuS[53]. In addition, the high-resolution S 2p XPS spectra present two spin-orbit splitting double peaks for S $2p_{1/2}$ and S $2p_{3/2}$ which are concentrated at 161.5 and 162.7 eV[54–56], respectively. The aforementioned results suggest that the CuS cathode materials are successfully synthesized.

The morphology and structure information of CuS-C50 microsphere are obtained by field emission SEM (FESEM) and high-resolution TEM (HRTEM), as shown in Fig.2. It can be seen from Fig.2a and 2b that the synthesized CuS-C50 has complete nanoflower shape which is filled with voids. TEM image (Fig.2c) further shows the full view of the microsphere structure and edge portion of the sheet-like structure of the CuS-C50 material. Fig. 2d displays three crystallographic planes (102), (107) and (203) of CuS-C50 in selected area electron diffraction (SAED) pattern. HRTEM images (Fig. 2e and 2f) indicate a lattice stripe of 0.1902 nm corresponding to the crystalline spacing of CuS along (107) and a lattice stripe of 0.3049 nm corresponding to the crystalline spacing of CuS

along (102), demonstrating that the CuS-C50 has a high degree of crystallinity.

It is clear that the complete nanoflower structure of CuS-C50 was successfully synthesized by adding the surfactant CTAB and adjusting the proportion of anhydrous ethanol in the solvent to 50vol% . In order to reveal the effect of the CTAB in the process of synthesis, CuS-50 and CuS-P50 were prepared. XRD patterns of CuS synthesized at three different additive states are shown in Fig. 3. Similarly, the diffraction peaks of CuS-50 and CuS-P50 are in perfect agreement with the standard peaks of hexagonal CuS. The CuS-50 and CuS-P50 microspheres are obtained by FESEM (Fig.4). Compared with the CuS-C50, both of CuS-50 and CuS-P50 do not have obvious nanoflower shape, and they only have dense and relatively smooth surface, which illustrates that the surfactant CTAB is a crucial factor for the formation of nanoflower shape of CuS-C50 materials.

The molecular structure of surfactant CTAB is shown in Fig. 5a. During the hydrothermal reaction, the hydrophilic group $-(H_3C)N^+$ decomposed by CTAB in the solvent attaches to the crystalline surface of CuS, so the hydrophobic film layer formed on the crystalline surface hinders the growth
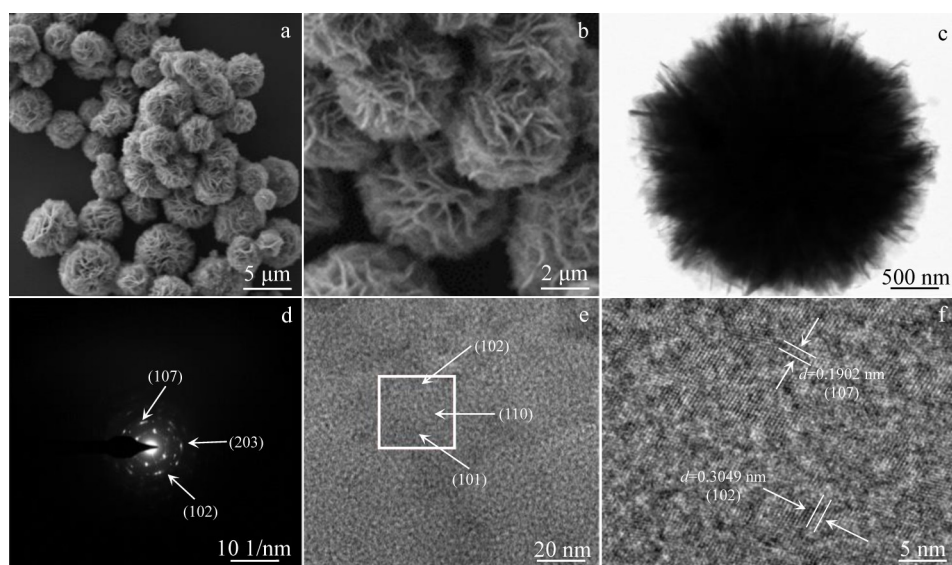
Fig.2 SEM images (a–b), TEM image (c), SAED pattern (d), and HRTEM images (e–f) of CuS-C50
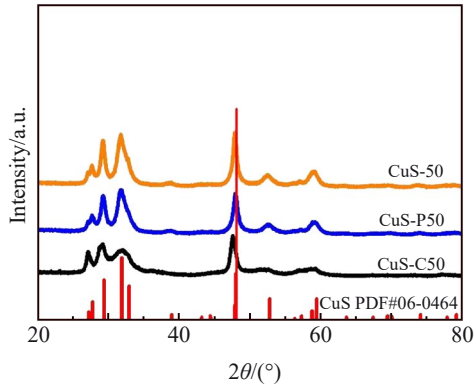
Fig.3　XRD patterns of CuS-50, CuS-P50 and CuS-C50

perpendicular to the surface and promotes the growth parallel to the crystalline surface, thus forming the specific nanoflower structure (Fig.5b)[57].

Fig. 6 shows CV curves, presenting charge and discharge tests results of CuS-C50 as magnesium ion batteries cathode in APC/THF electrolyte. The CV curves (Fig.6a) of CuS-C50 are measured in a voltage window from 0 V to 2.0 V, and the scanning rate is 0.2 mV/s. It can be seen that there are two oxidation peaks in the process of discharge, which are located at 0.9 and 1.4 V. With the increase in number of cycles, the oxidation peak gradually moves to the position of higher potential, and the peak current also gradually increases. Whereas, during the process of charge, the reduction peak moves to the lower potential with the increase in number of
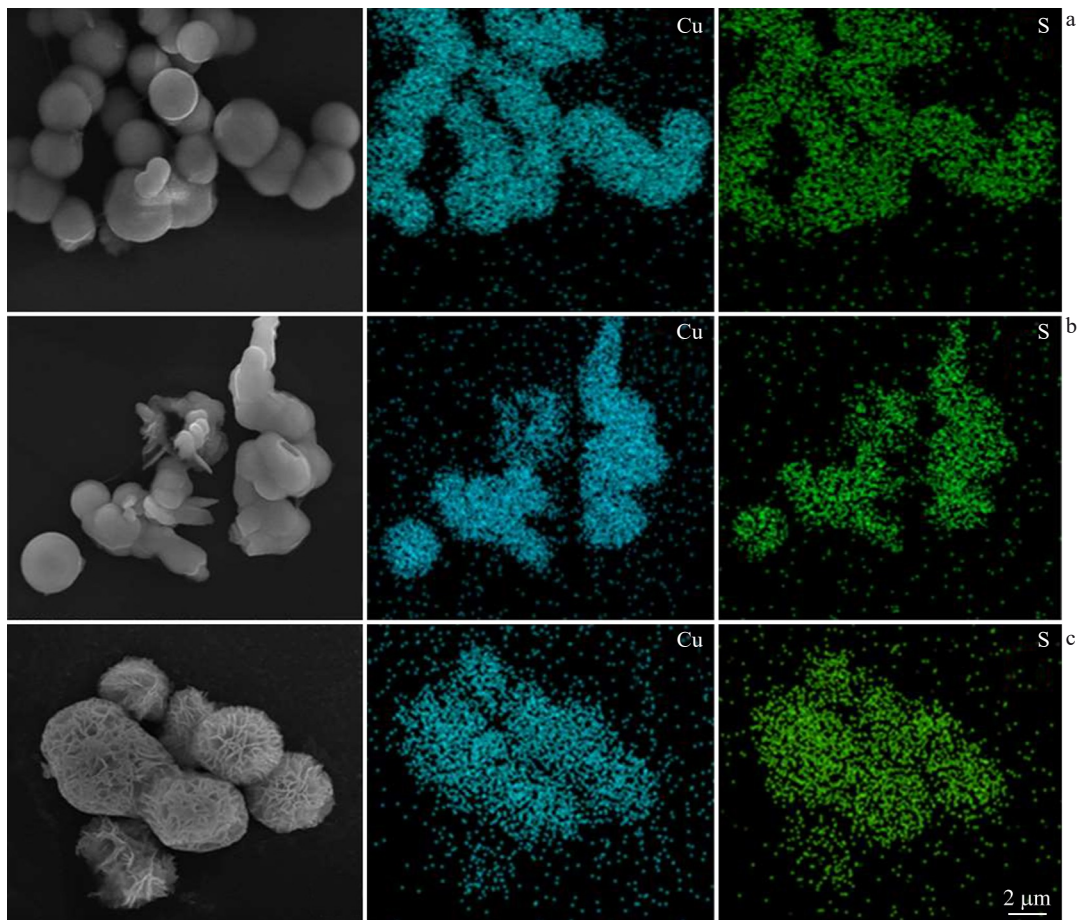
Fig.4　Structure and morphology characterizations: (a) CuS-50, (b) CuS-P50, and (c) CuS-C50

cycles. The changes of oxidation peaks and reduction peaks illustrate that as the number of cycles increases, the polarity of CuS-C50 decreases, whereas the discharge capacity of the battery increases gradually. The charge and discharge curves of the CuS-C50 with the current density of 50 mA/g are shown in Fig. 6b and 6c. There are two obvious discharge plateau areas, which are 1.0 and 1.5 V. The charge and discharge voltage profiles have relatively low specific capacity at the first several cycles, and the specific capacity increases first and then decreases as the reaction progress.

Before 30 cycles, the specific capacity increases, up to about 331.19 mAh/g. With the increase in number of cycles, the curves of specific capacity have a decreasing trend. After 50 cycles, the final specific capacity is 168.89 mAh/g. It indicates that the increase in active site of electrochemical reaction can improve specific capacity. In the early cycles, the nanoflower structure of CuS-C50 can provide many specific surface areas to electrochemical reaction. However, a little Mg^{2+} cannot be removed after embedding in the cathode as the discharge and charge process continues, eventually causing
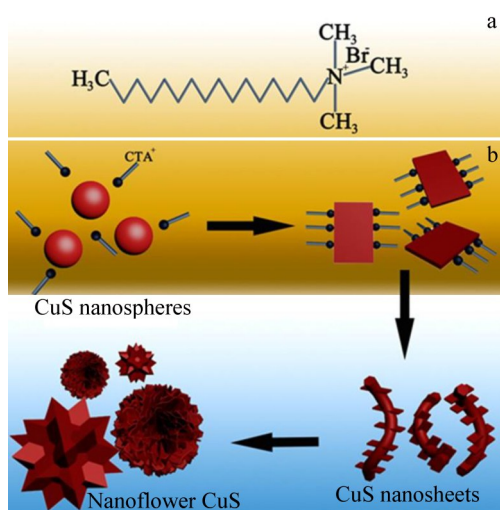
Fig.5 Structural formula of CTAB (a) and schematic diagram of formation process of nanoflower CuS (b)

the decrease in free-moving Mg^{2+}. Therefore, the specific capacity decreases from 331.19 mAh/g to 168.89 mAh/g (Fig. 6c). In addition, some Mg^{2+} cannot be removed from the positive electrode during the cycle, also resulting in a low reversibility of the redox reaction of the battery. Eventually, the specific charge capacity of the battery is much greater than the specific discharge capacity. The electrochemical impedance of CuS-C50 with difference cycles (0, 1 and 20 cycles) is measured by EIS (Fig. 7). The diameter of capacitive loops has a significant decreasing trend as the number of cycles increases, which may be attributed to more active sites for electrochemical reaction. SEM images of CuS-C50 after cycles are shown in Fig. 8. Large areas of nanoflower structure

can be observed on CuS-C50 in the early stage. When the number of cycles is more than 50, the nanoflower structure is collapsed completely, causing the decrease in the specific capacity and the number of active sites. Meanwhile, Fig. 6f shows the rate capability of CuS-C50 under 56, 112, 280, 560, and 56 mA/g current densities. The specific capacity of CuS-C50 is 278.6 mAh/g after 20 cycles at initial 56 mA/g, and when the current density gradually increases to 560 mA/g, the specific capacities are about 235.7, 114.1 and 15.4 mAh/g at current densities of 112, 280, 560 mA/g, respectively. When the current density is recovered back to 56 mA/g after 50 cycles, the specific capacity is about 248.99 mAh/g, which only decreases by 26.91 mAh/g from the initial specific capacity at 56 mA/g, suggesting that CuS-C50 has good rate capability. In addition, the Coulombic efficiency of CuS-C50 shows no significant decrease with the increase in the number of cycles and remains above 95%. The charge and discharge profiles at different current densities are shown in Fig. 6e. With the increase in current density, the discharge platform voltage of CuS-C50 decreases and the charge platform voltage increases, causing the increase in polarization of the batterie and the decrease in specific capacity (Fig. 6d). The cycling performance of CuS-C50 cathode in APC/THF electrolyte is tested at 200 mA/g (Fig. 6d). It can be seen that the specific capacity of CuS-C50 is maintained between 100 and 200 mAh/g. Even after 50 cycles, the specific capacity is still maintained at 136.92 mAh/g, which corresponds to 77.8% of the maximum capacity (175.88 mAh/g). The CuS-50 and CuS-P50 were tested by charge and discharge tests at 50 mA/g current density (Fig. 9). It can be seen that CuS-50 has a terrible specific capacity, whose initial specific capacity is less than 1 mAh/g and there is no significant increase trend. After adding surfactant PVP, the CuS-P50 has no obvious
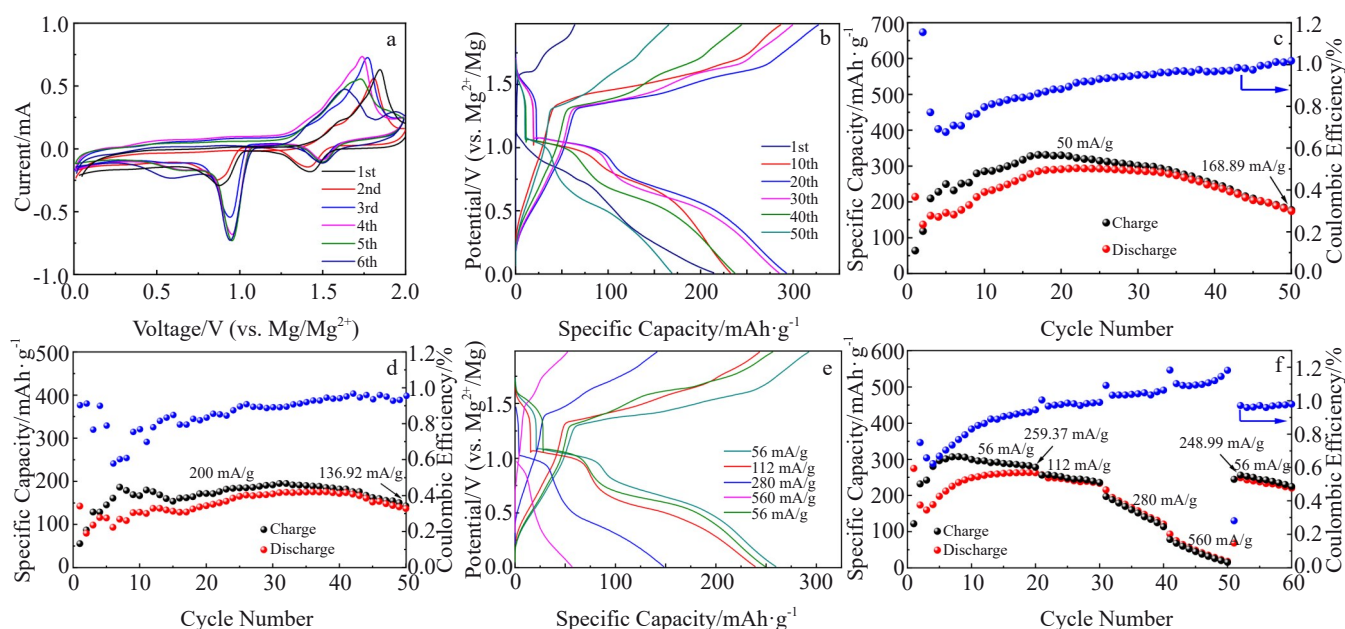
Fig.6 CV curves at different cycles (a); voltage profiles for cycling at 50 mA/g (b); specific capacities and Coulombic efficiency at 50 mA/g (c); rate capability under different current densities (d); voltage profiles at different current densities (e); cycling performance at 200 mA/g (f)
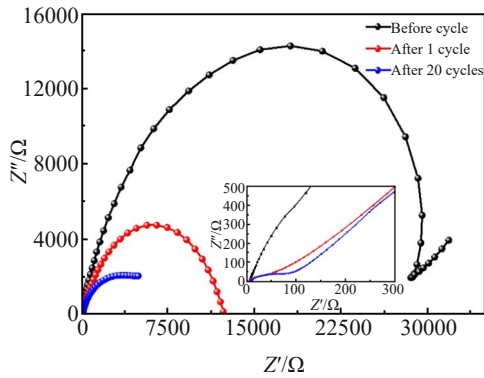
Fig.7 EIS results of CuS-C50 with difference cycles

improvement of charge and discharge performance, whose specific capacity remains at 2−3 mAh/g. The more complete the nanoflower CuS material, the larger the specific surface area, which can provide more active sites, and reduce the barriers of Mg^{2+} moving. Therefore, it can be inferred that synthesized CuS-C50 has excellent charge and discharge

performance, which may be a great cathode material for magnesium ion batteries.

To further expose the Mg^{2+} storage behavior of CuS-C50 cathode, ex-situ XRD was conducted at different discharge and charge states (Fig. 10a – 10b). The CuS-C50 electrode presents obvious diffraction peaks of CuS. The characteristic peaks of CuS start to diminish, whereas the peaks of MgS and Cu_2S start to appear during discharge to 1.0 V. It indicates that part of CuS is converted to Cu_2S and MgS. The characteristic peaks of MgS and Cu_2S are more obvious with the voltage of 0.01 V, and CuS is further transformed into MgS and Cu_2S. During the process of charge, the characteristic peaks of CuS reappear, whereas the peaks of Cu_2S and MgS disappear, which demonstrates that electrochemical reaction to generate CuS is reversible. Therefore, the electrochemical reaction in the process of charge and discharge are as follows:

$$2CuS + Mg^{2+} + 2e^- \leftrightarrow Cu_2S + MgS \tag{1}$$

$$2Cu_2S + Mg^{2+} + 2e^- \leftrightarrow 2Cu + MgS \tag{2}$$

Fig. 10c shows HRTEM image and the elemental distri-
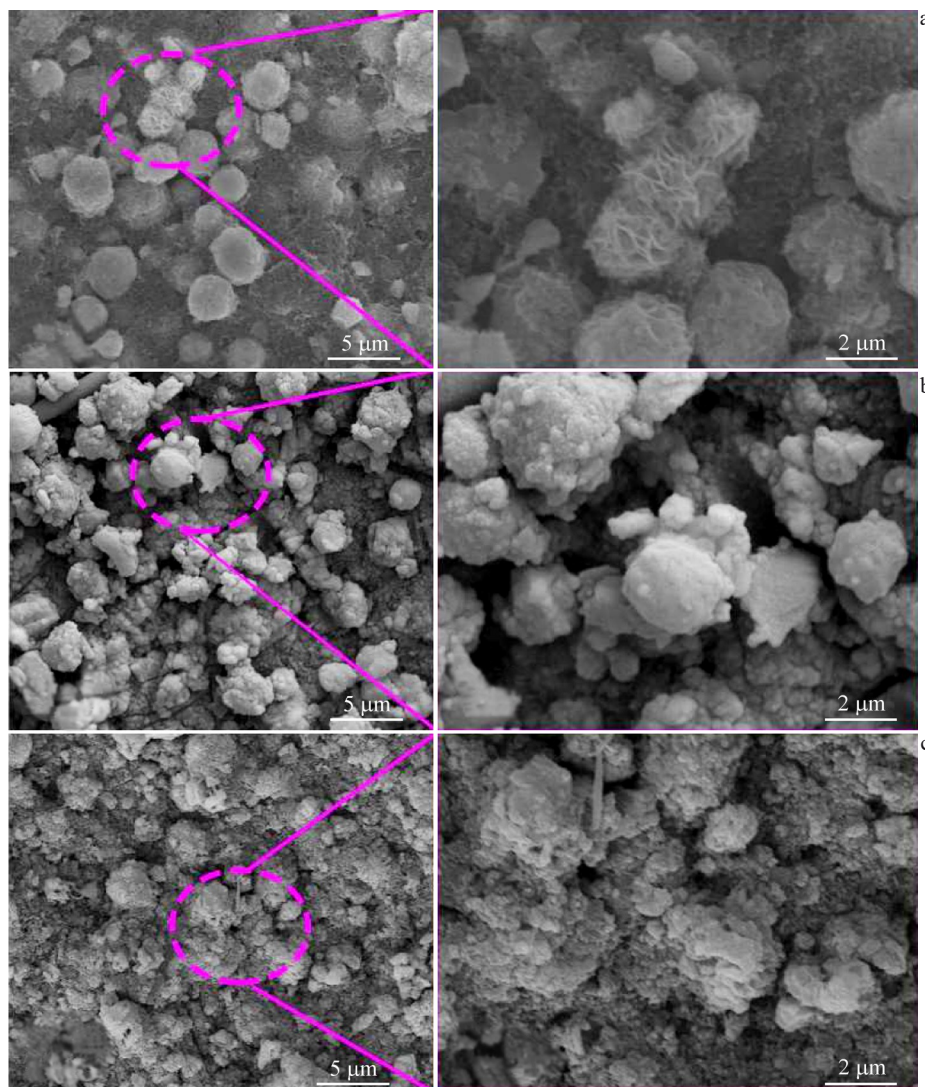
Fig.8 SEM images of CuS-C50 at different states: (a) before cycle; (b) after 20 cycles; (c) after 50 cycles
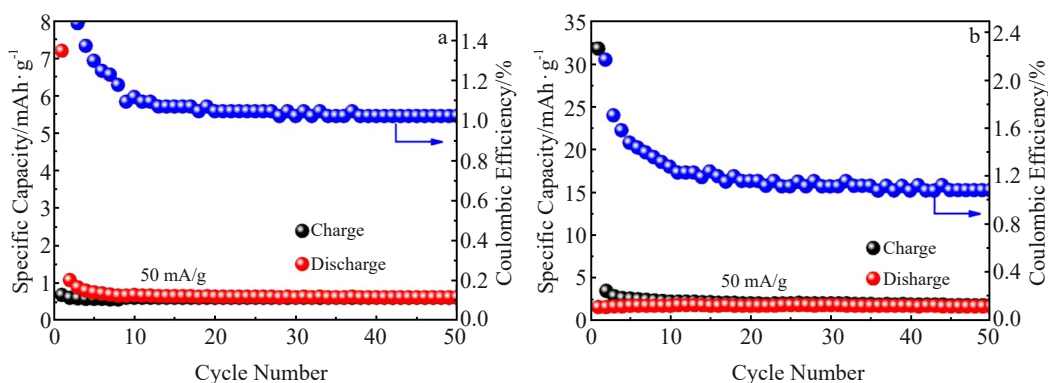
Fig.9 Cycling stability and corresponding Coulombic efficiency of CuS-50 (a) and CuS-P50 (b) at 50 mA/g
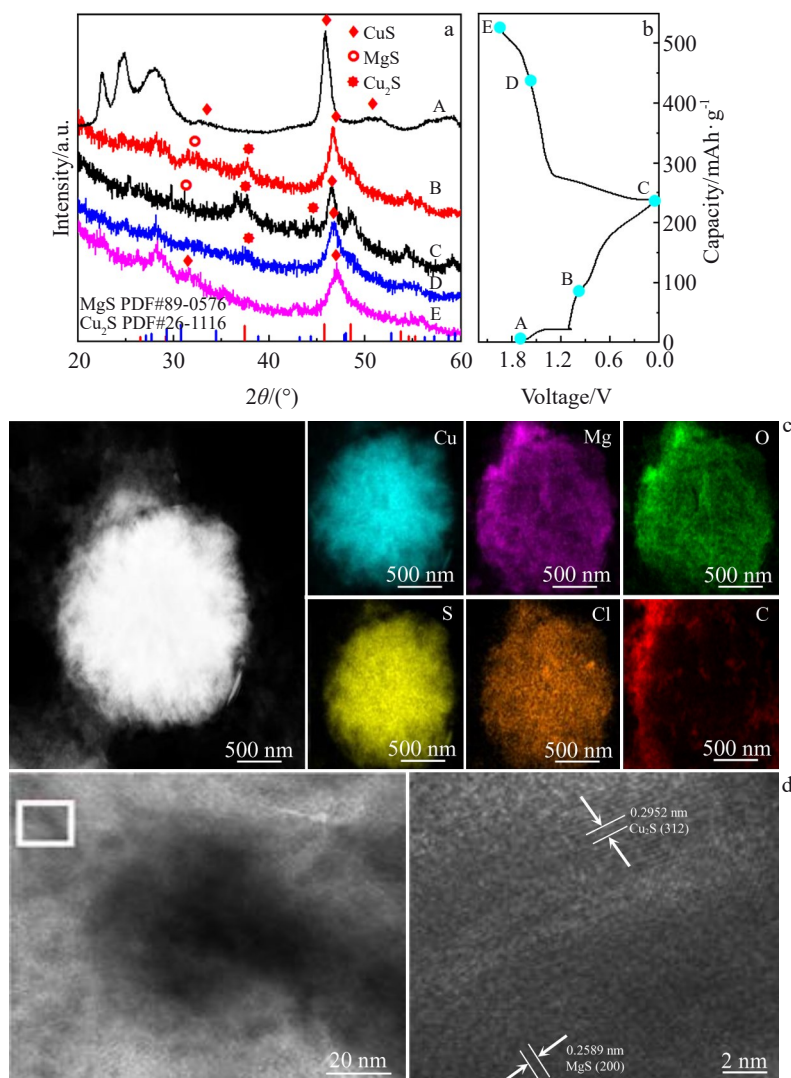
Fig.10 Results of ex-situ XRD (a–b), TEM image and corresponding EDS element mappings (c), and HRTEM images (d)

bution of CuS-C50 in the fully discharged state. It can be seen that CuS-C50 as a sphere has a flowerlike structure with a diameter of about 2 μm on the surface. And the elements Cu, Mg, S, Cl and O are distributed throughout the spherical structure. Fig. 10d shows HRTEM images of CuS-C50 in the fully discharged transient state. It can be seen that

there are (312) plane associated with Cu_2S and (200) plane associated with MgS. Therefore, there are still part of Cu_2S that cannot complete the reaction in Eq. (2) to produce monomeric Cu even in the fully discharged state, causing the Coulombic efficiency of CuS-C50 of the battery failing to reach 100%.

4 Conclusions

1) The CuS-C50 cathode material is synthesized by adding the surfactant CTAB and adjusting the percentage of ethylene glycol to 50vol% in the hydrothermal process.

2) The synthesized CuS-C50, as the cathode material for magnesium ion batteries, has good charge and discharge performance in APC/THF, which exhibits a high specific capacity of 331.19 mAh/g at 50 mA/g current density. At 200 mA/g current density, it can also reach 175.88 mAh/g, and still keeps specific capacity of 136.92 mAh/g after 50 cycles.

3) The complete nanoflower structure has larger specific surface areas, which significantly improves the active sites for electrochemical reaction and decreases barriers for Mg^{2+} mobility in the charge and discharge process.

Reference

1   Mao M L, Gao T, Hou S *et al*. *Chemical Society Reviews*[J], 2018, 47(23): 8804

2   Wang S, Jiao S Q, Wang J X *et al*. *ACS Nano*[J], 2016, 11(1): 469

3   Shen Y L, Wang Y J, Miao Y C *et al*. *Advanced Materials*[J], 2023, 35(19): 2208289

4   Zhang Q, Hu Y B, Wang J *et al*. *Journal of Magnesium and Alloys*[J], 2021, 11(1): 192

5   Kravchyk K V, Widmer R, Erni R *et al*. *Scientific Reports*[J], 2019, 9(1): 7988

6   Tran D T, Zhang S S. *Journal of Materials Chemistry A*[J], 2015, 3(23):12240

7   Nayak P K, Yang L T, Brehm W *et al*. *Angewandte Chemie International Edition*[J], 2019, 57(1): 102

8   Goodenough J B, Park K S. *Journal of the American Chemical Society*[J], 2013, 135(4): 1167

9   Su S J, Huang Z G, NuLi Y N *et al*. *Chemical Communications*[J], 2015, 51(13): 2641

10   Pan B F, Feng Z X, Sa N *et al*. *Chemical Communications*[J], 2016, 52(64): 9961

11   Colpo P, Ruiz A, Ceriotti L *et al*. *Advances in Biochemical Engineering/Biotechnology*[J], 2010, 117: 109

12   Li Y Q, Zuo P J, Li R N *et al*. *Journal of Energy Chemistry*[J], 2019, 37: 215

13   Carter T J, Mohtadi R, Arthur T S *et al*. *Angewandte Chemie International Edition*[J], 2014, 53(12): 3173

14   He X Q, Cheng R Q, Sun X Y *et al*. *Journal of Magnesium and Alloys*[J], 2023, 11(12): 4359

15   Aurbach D, Lu Z, Schechter A *et al*. *Nature*[J], 2000, 407: 724

16   Huie M M, Bock D C, Takeuchi E S *et al*. *Coordination Chemistry Reviews*[J], 2015, 287: 15

17   Reddygunta K K R, Kumar B D. *International Journal of Energy Research*[J], 2022, 46(15): 22285

18   Montenegro C T, Peter J F, Baumann M *et al*. *Journal of Energy Storage*[J], 2021, 35: 102053

19   Toshihiko M, Kiyoshi K. *Journal of the Electrochemical Society*[J], 2017, 5: 444

20   Sun X Q, Bonnick P, Duffort V *et al*. *Energy & Environmental Science*[J], 2016, 9(7): 2273

21   Zhou L M, Xiong F Y, Tan S S *et al*. *Nano Energy*[J], 2018, 54: 360

22   Tao G, Hou S Y, Wang F *et al*. *Angewandte Chemie International Edition*[J], 2017, 56(43): 13526

23   Tan X P, Guo G L, Wang K D *et al*. *Journal of Nanomaterials*[J], 2022, 12(15): 2530

24   Wang J S, Zhang Y Q, Liu G *et al*. *Small*[J], 2023, 20(6): 2304969

25   Setiawan D, Lee H, Bu H *et al*. *Small Structures*[J], 2024, 5(1): 2300228

26   Li H Q, Qi J T, Tang Y C *et al*. *Nano Letters*[J], 2024, 24(22): 6465

27   Zhang Z H, Dong S M, Cui Z L *et al*. *Small Methods*[J], 2018, 2(10): 1800020

28   Eames C, Islam M S. *Journal of the American Chemical Society*[J], 2014, 136(46): 16270

29   Gu X N, Zheng Y F. *Frontiers of Materials Science in China*[J], 2010, 4: 111

30   Song J X, Xu T, Gordin M L *et al*. *Advanced Functional Materials*[J], 2013, 24(9): 1243

31   Muldoon J, Bucur C B, Gregory T. *Chemical Reviews*[J], 2014, 114(23): 11683

32   Sheha E. *Graphene*[J], 2014, 3(3): 36

33   Nam K W, Kim S, Lee S *et al*. *Nano Letters*[J], 2015, 15(6): 4071

34   Tepavcevic S, Liu Y, Zhou D H *et al*. *ACS Nano*[J], 2015, 9(8): 8194

35   Le T S, Hoa T H, Truong D Q. *Journal of Electroanalytical Chemistry*[J], 2019, 848: 113293

36   Gu Y P, Katsura Y, Yoshino T *et al*. *Scientific Reports*[J], 2015, 5(1): 12486

37   Li Y J, Ma G Y, Song J M *et al*. *Science China-Chemistry*[J], 2021, 51(6): 782

38   Tao Z L, Xu L N, Gou X L *et al*. *Chemical Communications*[J], 2004, 40(18): 2080

39   Hennequart B, Deschamps M, Chometon R *et al*. *ACS Applied Energy Materials*[J], 2023, 6(16): 8521

40   Bonnick P, Sun X Q, Lau K C *et al*. *The Journal of Physical Chemistry Letters*[J], 2017, 8(10): 2253

41   Wang Y R, Liu Z T, Wang C X *et al*. *Advanced Materials*[J], 2018, 30(32): 1802563

42   Machani T, Rossi D P, Golden B J *et al*. *Chemistry of Materials*[J], 2011, 23(24): 5491

43   Zhang Q, Hu Y B, Wang J *et al*. *The Journal of Physical Chemistry C*[J], 2021, 125(36): 19673

44   Chaki S H, Tailor J P, Deshpande M P. *Materials Science in Semiconductor Processing*[J], 2014, 27: 577

45   Radich E G, Dwyer R, Kamat P V. *The Journal of Physical*

Chemistry Letters[J], 2011, 2(19): 2453

46 Lai C H, Huang K W, Cheng J H *et al. Journal of Materials Chemistry*[J], 2010, 20(32): 6638

47 Wu M Y, Zhang Y J, Li T *et al. Nanoscale*[J], 2018, 10(26): 12526

48 Shen J W, Zhang Y J, Chen D *et al. Journal of Materials Chemistry A*[J], 2019, 7(37): 21410

49 Du C L, Zhu Y Q, Wang Z T *et al. ACS Applied Materials & Interfaces*[J], 2020, 12(31): 35035

50 Huang J Q, Zhu Y Q, Du C L *et al. Electrochimica Acta*[J], 2021, 388: 138619

51 Shen Y L, Zhang Q, Wang Y J *et al. Advanced Materials*[J], 2021, 33(41): 2103881

52 Du A B, Zhang Z H, Qu H T *et al. Energy & Environmental Science*[J], 2017, 10(12): 2616

53 Perry D L, Taylor J A. *Journal of Materials Science Letters*[J], 1986, 5(4): 384

54 Raj S I, Jaiswal A, Uddin I. *RSC Advances*[J], 2020, 10(24): 14050

55 Nayak A, Tsuruoka T, Terabe K *et al. Applied Physics Letters*[J], 2011, 98(23): 233501

56 Zhou Q X, Fang Z. *RSC Advances*[J], 2014, 4(15): 7471

57 Zhang Y, Xie J J, Han Y L *et al. Advanced Functional Materials*[J], 2015, 25(47): 7300

纳米花状CuS作为镁离子电池正极材料

何元泰[1]，吴　量[1,2]，史永安[3]，钟志永[1]，姚文辉[1,2]，潘复生[1,2]

(1. 重庆大学 材料科学与工程学院 国家镁合金材料工程技术研究中心，重庆 400044)

(2. 重庆大学 机械传动国家重点实验室，重庆 400044)

(3. 池州市质量监督检验研究院，安徽 池州 247100)

摘　要：在水热合成过程中加入表面活性剂十六烷基三甲基溴化铵（CTAB），调节乙二醇的用量为50vol%，合成了镁离子电池正极材料CuS-C50。结果表明：CuS-C50具有完整的纳米花状结构，在氯化铝-季戊四醇四甲醚/四氢呋喃（APC/THF）电解液中，当电流密度为50 mA/g时，其比容量高达331.19 mAh/g；当电流密度为200 mA/g时，其比容量在50次循环后仍保持136.92 mAh/g。形貌表征结果表明，完整的纳米花状结构可以提供更多的活性位点，减少Mg^{2+}的移动障碍，最终提高镁离子电池CuS正极材料的充放电性能。

关键词：硫化铜；纳米花；镁离子电池；CTAB；水热合成

作者简介：何元泰，男，1996年生，博士生，重庆大学材料科学与工程学院国家镁合金材料工程技术研究中心，重庆 400044，E-mail：1677573729@qq.com